JOURNAL OF MATERIALS SCIENCE **34** (1999) 5187–5197

Microstructural evolution during transient liquid-phase bonding in a Ni-base superalloy/sapphire fiber composite

M. W. TSENG, D. B. WILLIAMS*
Department of Materials Science and Engineering, Lehigh University, Bethlehem, PA 18015, USA

K. K. SONI‡, R. LEVI-SETTI
The Enrico Fermi Institute, The University of Chicago, Chicago, IL 60637, USA
E-mail: dbw1@lehigh.edu

Transient-liquid-phase (TLP) bonding was used to fabricate a Haynes 230 Ni-base superalloy/sapphire fiber composite for high-temperature applications. Boron was used as a melting-point depressant for the Ni, to aid superalloy infiltration of the fibers. Preliminary study of the composite indicated an incomplete TLP bonding cycle. Therefore, microstructural and microchemical analyses were carried out to determine the TLP bonding mechanism. It was found that the TLP process did not occur under local thermodynamic equilibrium conditions at the solid/liquid interfaces, contrary to the primary assumption of conventional models, so a modified model for TLP bonding is proposed. The main differences between the proposed and the conventional models are: (a) the concentration of the melting-point depressant increases with time during isothermal solidification, (b) extensive boride segregation at γ grain boundaries and boride precipitation occurs within γ grains adjacent to the interlayer in the initial composite assembly, (c) because of the relatively high boron concentration in the interlayer, the TLP bonding cycle was incomplete, resulting in residual-liquid borides. To achieve ideal TLP bonding, four modifications are recommended: (i) use less boron, (ii) use finer sapphire fibers, (iii) create smaller initial grain sizes in the γ matrix and (iv) increase the homogenization time.

1. Introduction

As part of the National Aerospace Plane (NASP) program, a Ni-base superalloy/sapphire fiber-composite system has been developed by Rockwell International Corporation for very high-temperature and high-strength applications, such as turbine-engine components (vanes, blades, etc.) [1]. Theoretically, according to the rule of mixtures, Ni-base alloys reinforced with single-crystal Al_2O_3 (sapphire) fibers or whiskers have promising properties as structural materials used under harsh conditions. Consequently, these composites received substantial attention during the mid-1960s to mid-1970s [2]. However, because of (i) the difficulties of bonding brittle sapphire fibers with ductile Ni-base alloys, and (ii) the fiber degradation at high temperatures, the early attempts to develop this composite system were not successful. The composite system had unexpectedly poor mechanical properties (e.g. low tensile strengths and high creep rates [2]).

To date, advanced directionally solidified and single-crystal Ni-base superalloys are used at their strength limits [3]. To meet the requirements for the next-generation aircraft, a different composite fabrication technique: transient-liquid-phase (TLP) bonding [1, 4–7] was applied to the Ni alloy-Al_2O_3 system. The TLP bonding is an ancient technique (dating back to the sixteenth century [8]) used in the welding industry to join materials such as Ni-base alloys [9–13], stainless steels [14, 15], Al-base alloys [16–18], and other alloys, as well as intermetallics [19–21]. The TLP bonding requires the use of a melting-point depressant to partially liquefy the matrix phase, permitting easy penetration between the fibers. Early attempts at TLP fabrication have been fairly successful in Al-alloy metal-matrix composites (Al-MMCs) since the early 1990s [4, 6]. It was anticipated, on the basis of the early Al work, that using TLP bonding to reinforce a Ni-base superalloy with sapphire fibers would have the following advantages: (i) cleaning of the fibers by the transient-liquid metal, (ii) less damage to the fibers from the lower clamping pressure, (iii) synergism with "laminated" composite design (foil/fibers/foil), (iv) a

* Author to whom all correspondence should be addressed.
‡ *Present address:* Corning Incorporated, Science & Technology Group, Corning, NY 14831, USA.

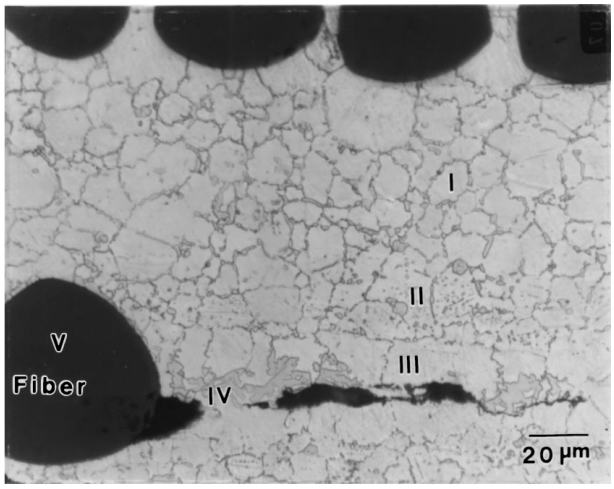

Figure 1 Light optical micrograph showing the heterogeneous microstructure of an as-fabricated region of the Haynes 230 superalloy/sapphire composite (etchant: aqua regia). The five principal regions of the microstructure are indicated.

homogeneous matrix structure with no trace of the melting-point depressant after bonding, (v) lower bonding temperature due to the presence of the TLP, (vi) less bonding time because of rapid liquid-state diffusion, and (vii) a higher operating temperature than bonding temperature; i.e., the composite would be fabricated at a relatively low temperature but used at a much higher temperature [5, 8].

Because the conventional TLP bonding models only deal with binary systems [8], the optimum bonding parameters (such as temperature, pressure, time, and interlayer composition) in multi-element systems can only be obtained experimentally. In this particular case, the as-fabricated TLP superalloy/sapphire composite has an inhomogeneous microstructure (see Fig. 1), indicating an incomplete TLP bonding cycle. Therefore, microstructural and microchemical analyses were carried out to understand the mechanism and kinetics of the TLP bonding in this composite. The results described in this paper permit changes to be proposed, which should improve future processing of the composite.

The aim of this study, therefore, is to understand the role of boron (used as a melting-point depressant for Ni) in the TLP bonding process. Boron is difficult to detect and analyze using conventional X-ray microanalytical techniques, so the classical crystal spectrometry studies in the electron probe microanalyzer (EPMA) were augmented by scanning ion microscopy/secondary ion mass spectrometry (SIM/SIMs) studies. Such ion-based characterization tools permit relatively easy detection and mapping of the boron distribution, at higher spatial resolution than the EPMA.

2. Conventional TLP bonding models

In this paper, only a brief review of the conventional TLP bonding models will be given; interested readers can refer to refs. [8, 22, 23]. Following the approach applied by Tuah-Poku and coworkers [23], the mechanism of the TLP bonding process in a binary-alloy system is usually described by illustrating a phase diagram as shown in Fig. 2. For simplicity, an interlayer of pure element B is used to join two pieces of pure element A; element B (an appropriate symbol, since boron is used in this study) serves as the melting-point depressant for the matrix element, A. In practice, in most cases, an interlayer with a eutectic composition is used, rather than a pure element, to shorten the overall bonding time. The microstructural evolution and the associated concentration profile of solute B across the bonding region are also illustrated in Fig. 2. According to Fig. 2, the TLP bonding process can be broken down into six stages: (a) initial bonding assembly (T_B is the bonding temperature), (b) dissolution of the interlayer due to interdiffusion of A and B during heating up to T_B and holding at T_B, (c) widening and homogenizing of the liquid interlayer to maximum width, (d) shrinkage and solidification of the liquid interlayer due to loss of solute B, (e) complete solidification at T_B and (f) homogenization of the bond region.

It should be noted that in TLP bonding, the solidification process occurs isothermally at T_B (Figs. 2d and e). The driving force for the bonding to proceed is the concentration gradient of solute B between the interlayer and the parent metal. Theoretically, a homogenous microstructure can be obtained by holding the composite for a sufficient time at a high enough temperature during the TLP bonding process. While some grain growth may well be expected during the homogenization stage, this is not shown in Fig. 2. Ideally, no residue of the melting-point depressant or the interlayer phase remains after bonding, as shown schematically in Fig. 2f.

It has also been noted that the dissolution, widening and homogenization of the interlayer usually take only a few minutes (because the liquid-state diffusion is rapid), while the controlling stages of the TLP bonding, isothermal solidification of the liquid and homogenization of the bond region, take hours to complete (under solid-state diffusion control). Several other models have attempted to quantify the total time required to complete the TLP bonding [8, 12, 23]. As pointed out by MacDonald and Eagar [8], the TLP bonding models dealing with the kinetics of the process often overestimate the total time required. Tuah-Poku *et al.* suggested that this over-estimation is probably due to the assumption of a simplified "planar" liquid/solid moving interface, whereas a curved or ledge-like interface may be involved in reality [23]. According to Li *et al.* [7], the bonding process was faster in the actual joints because solute transfer was promoted by grain-boundary diffusion in the parent metal. Another possible explanation given by MacDonald and Eagar [8] is that the liquid interlayer leaked out of the joint region during bonding.

It should be noted that the mechanism of the solid front advancing into the liquid interlayer is not clear yet [8]. Therefore, to better understand the mechanism, it is necessary to correlate the diffusion profile of the solute with the associated microstructure; i.e. understanding the redistribution of boron in the composite is crucial.

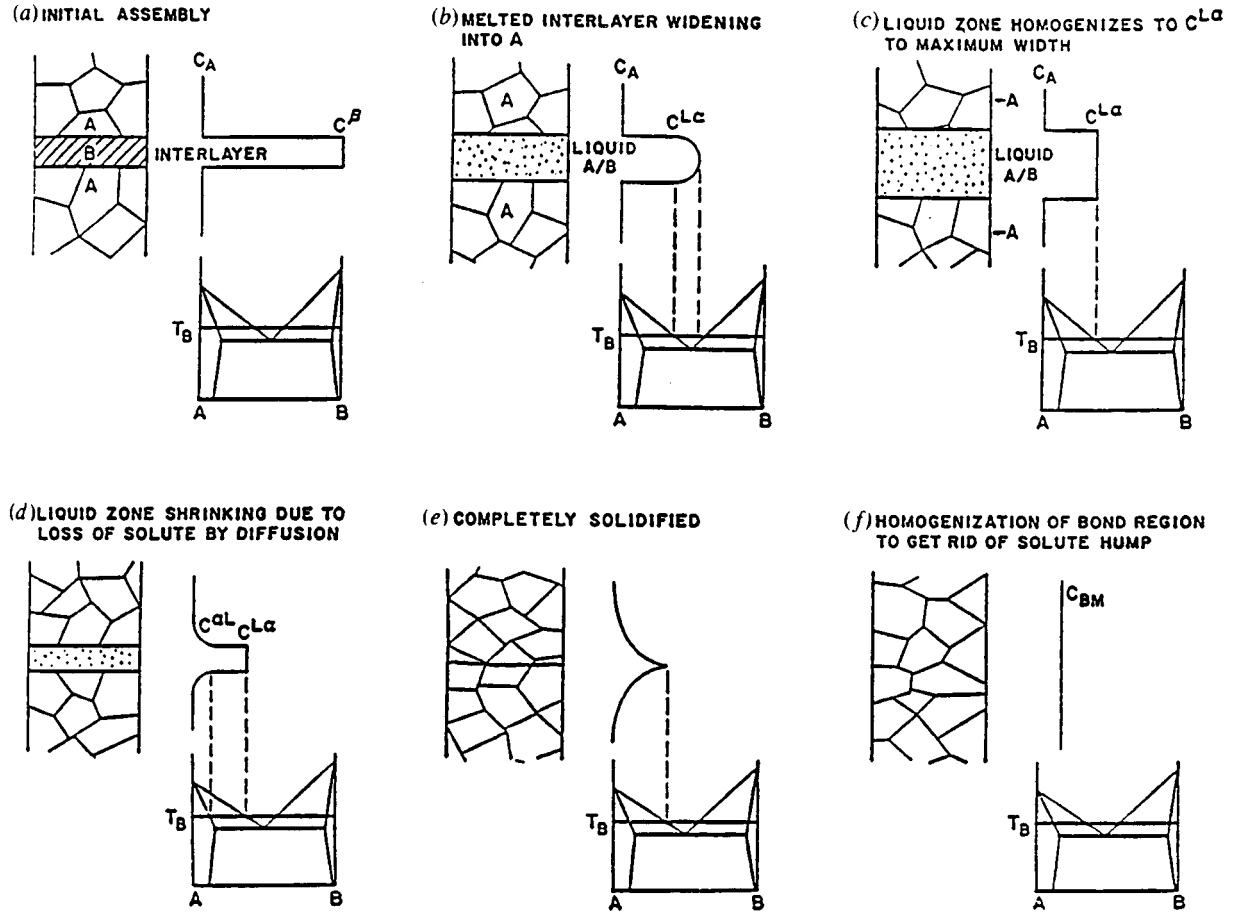

Figure 2 Schematic illustration of the mechanism of TLP bonding process (from Tuah-Poku *et al.*, 1988, Fig. 2 [26], reproduced with permission from ASM International, Materials Park, OH).

3. Material and characterization techniques

3.1. Composite processing conditions

The composite investigated in this study was a Haynes 230 Ni-base superalloy matrix, reinforced with single crystal Saphikon α-Al_2O_3 (sapphire) fibers. The composite was fabricated at Rockwell by TLP bonding, which involved hot isostatic pressing at 1200 °C, at 2 ksi (~14 MPa), for two hours, in vacuum. The preform arrangement of the composite is illustrated in Fig. 3. A thin layer of powder mixture was placed between an array of sapphire fibers and Haynes 230 foil. The interlayer powder mixture was Haynes 230, doped with 3.4 wt % boron. The nominal chemical composition of the Haynes 230 is listed in Table I. Compared with other Ni-base superalloys, Haynes 230 has a rather simple microstructure; the well-known strengthening phases γ' and γ'' are not present.

Ideally, upon heating to the bonding temperature, 1200 °C, the boron-doped interlayer (which has a lower melting point) liquefies, and the liquid then fills in the gaps between fibers. With time, given the driving force of the boron concentration gradient between the liquid and the superalloy matrix, boron diffuses back into the matrix. Simultaneously, the liquid solidifies isothermally at the bonding temperature.

TABLE I Chemical composition of Haynes 230 Ni-base superalloy (wt %)

Ni	Cr	W	Mo	Fe	Co	Mn	Si	Al	C	La	B
Balance	22	14	2	3	5	0.7	0.5	0.3	0.1	0.04	0.015

3.2. Characterization techniques

The chemistry of the as-fabricated composite was analyzed by electron-probe microanalysis (EPMA) and secondary-ion mass spectrometry (SIMS). EPMA was performed to obtain quantitative elemental distributions of boron and other alloying elements. The JEOL 733 electron microprobe is equipped with four wavelength-dispersive spectrometers (WDS) and a Si(Li) energy-dispersive spectrometer (EDS), and is designed for chemical analysis of bulk specimens with a spatial resolution of 1–2 μm. A 15 keV electron beam with a current ranging from 30–60 nA was used to conduct point analyses, line scans, and digital X-ray compositional maps. Quantitative X-ray analysis was performed by using pure-element standards as well as stoichiometric chemical compounds (such as Al_2O_3, Cr_3C_7, and B_4C) and a standard ZAF correction routine. Because the total ZAF correction is often >1.5 for the light elements of interest in this study, such as B, C, and O, errors of ~±50% relative are possible for these specific elements. (For heavier elements, typical errors are much less (<5%).) Therefore, to give a better picture

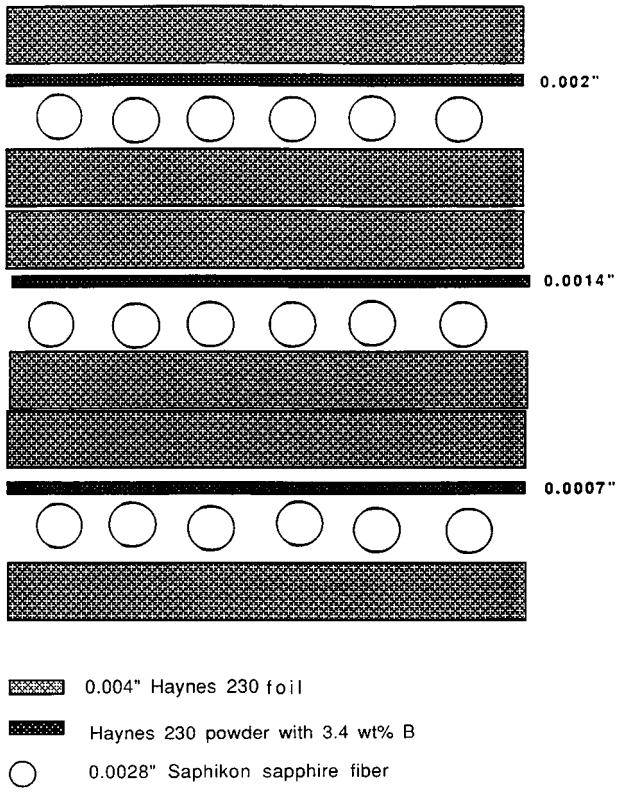

Figure 3 Schematic diagram of the preform arrangement used in the fabrication of the Haynes 230 superalloy/sapphire composite.

of the distribution of the lightest elements, the scanning ion microprobe (SIM) developed at the University of Chicago (UC) [24–26] was also used to obtain the elemental distributions within the composite. Combining a SIM system with SIMS offers higher lateral resolution (20–100 nm) than EPMA and excellent analytical sensitivity, but quantification is very difficult. Qualitative SIMS analyses were performed with an RF quadrupole or a magnetic-sector mass spectrometer. The UC SIM uses a primary gallium ion beam accelerator to 40 keV. The instrument is described in more detail in ref. [24], and its applications in the analysis of composites are discussed in refs. [25, 26]. The SIM/SIMS and EPMA complement one another, to give a good combination of quantitative analysis and high spatial resolution mapping.

4. Experimental results

The optical micrograph in Fig. 1 depicts the heterogeneous microstructure of the as-fabricated Haynes 230/sapphire composite. The microstructure can be broken down into five constituent regions, indicated on the micrograph. Region I is the alloy matrix with blocky borides segregated primarily along grain boundaries. Region II is similar to region 1, but with a high density of intragranular rod-like and/or globular boride precipitates. Region III is the γ phase (the austenitic matrix of the Haynes 230 alloy) resulting from the isothermal transient liquid solidification, which has a coarse-grain structure. Region IV is the "residual liquid" region, which is enriched with boron and solidified athermally. Region V is the sapphire fibers. The evidence for boron or boride distribution in the matrix is described as follows.

Fig. 4a–d are SIM compositional maps of region I in the as-fabricated composite: (4a) ion-induced secondary-ion image (ISI) topographic map, (4b) B^+ map, (4c) Al^+ map, and (4d) Mn^+ map. It is clear that, during fabrication, boron segregated to the grain boundaries while Al and Mn were depleted in the boron-rich grain-boundary precipitates. Using EPMA (Fig. 5), it was found that these grain-boundary borides are enriched with Cr, W, and Mo.

The fine intragranular precipitates (<1 μm) in region II were also identified as borides, as illustrated in Fig. 6: the SIM B^+ map. Fig. 6b clearly depicts the globular and rod-like boride precipitates (arrowed), while the EPMA maps barely reveal these fine borides as shown in Fig. 7a–d, demonstrating the higher spatial resolution of the SIM maps.

Fig. 8 shows the EPMA compositional profiles of B, Mo, Cr, and W across the matrix (from right to left: regions: I $\rightarrow$ II $\rightarrow$ III $\rightarrow$ IV $\rightarrow$ III). It is noted that B, Mo, Cr, and W have similar distribution tendencies (i.e. forming borides). The most important analysis in this study is that in region IV (the "residual liquid") the boron concentration ranges from 7–13 wt %, which is much higher than the initial boron concentration in the interlayer, i.e. 3.4 wt %.

5. Discussion

5.1. The TLP bonding mechanism in the composite

Combining the light optical microscopy observation (Fig. 1) with the SIMS and EPMA analyses (Figs 4–8), it is clear that boron diffused back into the metallic matrix primarily along grain boundaries, down the boron concentration gradient. The boron diffuses down the grain boundary rather than through the matrix because (1) the solubility of boron in the Ni-base superalloy matrix is near zero, according to the Ni-B binary phase diagram [27], and (2) the diffusivity of boron in the superalloy lattice is also low ($D = 1.8 \times 10^{-9}$ m^2/s, at 1200 °C [12]).

Because boron diffused mainly along the grain boundaries, it is very likely that boron wetted the grain boundaries once the local boron concentration exceeded the liquidus point of the Haynes 230-boron system. Therefore, the diffusion of boron was controlled by both solid-state and liquid-state diffusion during the bonding process. This observation may explain why the experimental bonding times were considerably shorter than the theoretically calculated values [8, 12, 23]. In the conventional TLP models, only the solid-state diffusion of the solute into the matrix is taken into account, while the evidence from this study clearly indicates that the solute might diffuse along the grain boundary via liquid-state diffusion.

Since region II was adjacent to the interlayer in the initial assembly, it is possible that region II was partially melted during the heating-up, interlayer-melting, and widening stages. If partial melting occurred, boron

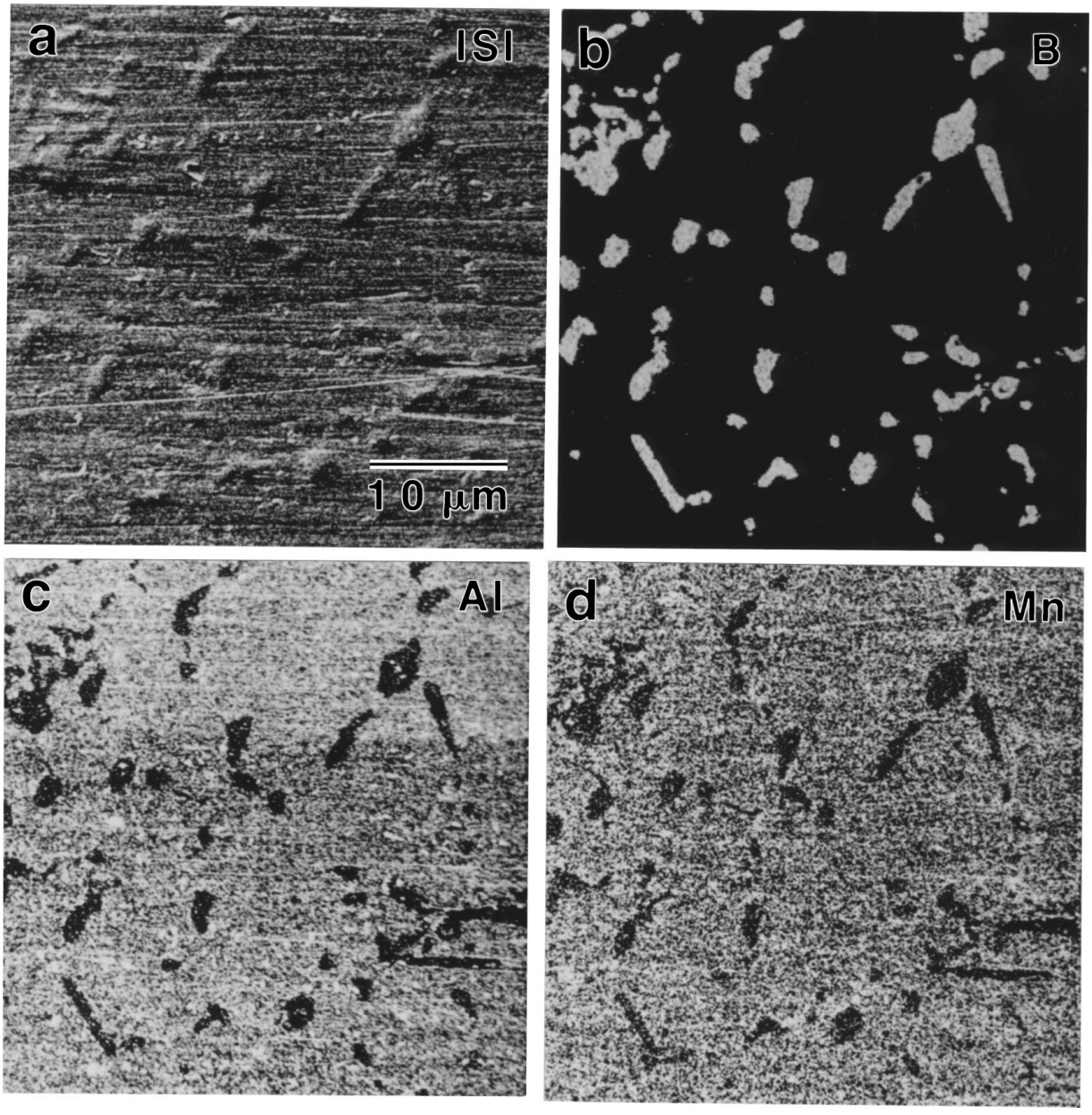

Figure 4 SIM images of an as-fabricated Haynes 230 superalloy/sapphire composite in region I (defined in Fig. 1): (a) ion-induced secondary ion (ISI) topographic map, (b) B^+ map, (c) Al^+ map, and (d) Mn^+ map. Note the enrichment of boron at grain boundaries, and the depletion of Al and Mn in the boron-rich grain boundary precipitates.

would have been able to diffuse easily into the region II. Therefore, because of the low solubility and lattice diffusivity of boron in the matrix, it is likely that region II was supersaturated with boron during the two hours of bonding time. Consequently, there are two possible mechanisms for the Cr-W-Mo boride precipitation within region II. First, on cooling, boron precipitated out of region II and formed borides. Second, during the bonding process, boride precipitation from the boron-supersaturated region II took place isothermally. It is also possible that the nucleation of borides started during the bonding process, and the growth of the boride precipitates followed during the cooling stages. Thus, the large number of intragranular borides in region II is explained.

Region III is mainly the FCC γ phase, and is the direct product of isothermal solidification of the liquid. The γ phase continued to form isothermally at the expense of the remaining boron-rich liquid; the liquid region continued to narrow until the solidus point of the Haynes 230-boron system had been reached. Ideally, with a sufficient time, all the liquid solidifies isothermally. Apparently, two hours of bonding time was not enough to complete the TLP bonding; some liquid was left after bonding (thus accounting for the "residual liquid" borides).

Because the boron concentration detected in region IV by EPMA (Fig. 8) is much higher than the starting boron concentration (3.4 wt %) of the interlayer, this region could not possibly be solid during bonding. The remaining liquid solidified athermally during the post-bonding cooling stages.

The increase of boron concentration in the interlayer is contrary to the general assumption of the conventional TLP bonding models. As illustrated in Fig. 2, the solute concentration in the interlayer should gradually

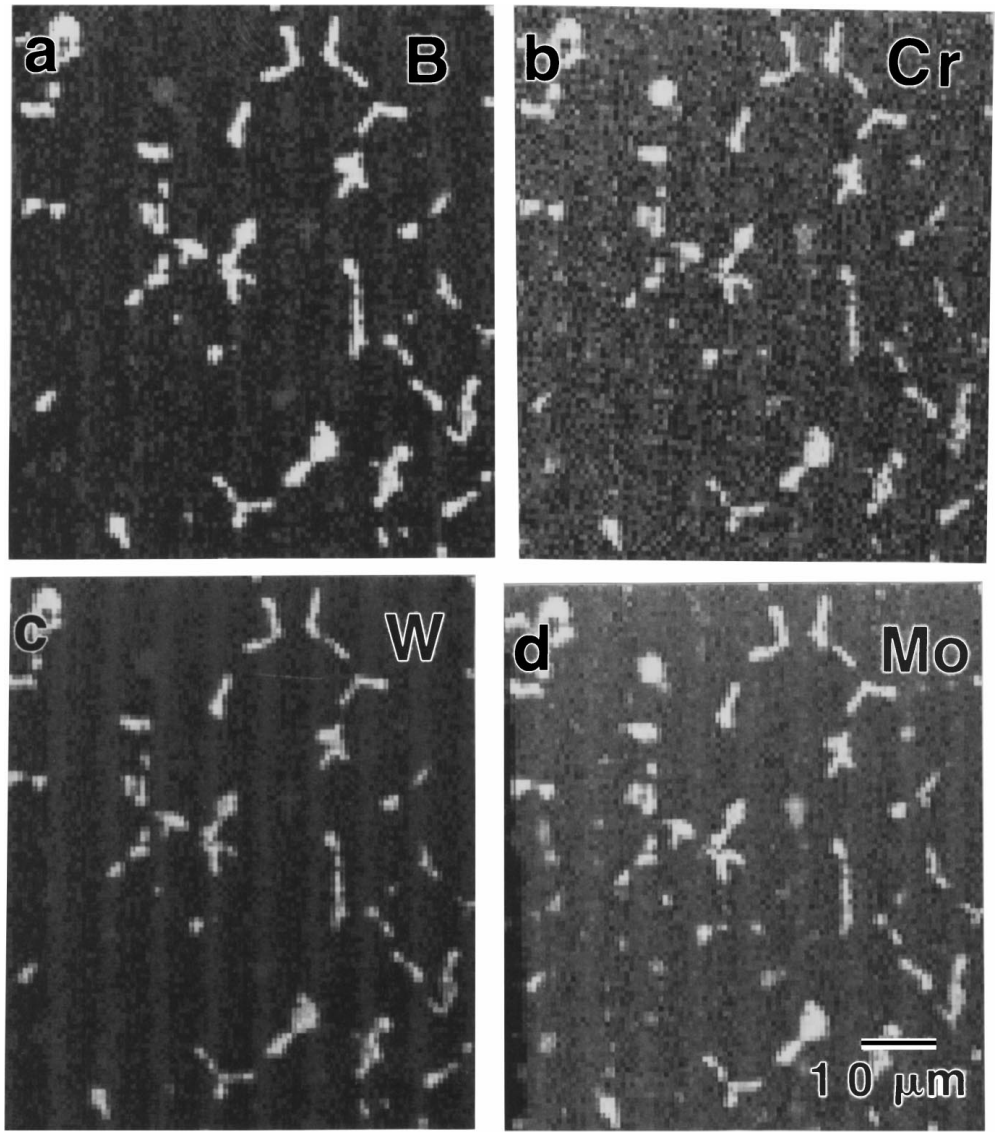

Figure 5 EPMA X-ray images of region I in an as-fabricated Haynes 230 superalloy/sapphire composite (similar area to that shown in Fig. 4): (a) B map, (b) Cr map, (c) W map, and (d) Mo map. Note that B, Cr, W, and Mo have similar distributions, and these elements form the grain-boundary borides in region I.

decrease as the bonding proceeds. It should be noted also that, at the isothermal solidification stage (Fig. 2d and e), the solute concentration is considered constant in the interlayer; i.e. local equilibrium is assumed at the liquid/solid interface (thus the compositions of the liquid and solid are dictated by the phase diagram).

In this study, however, it is evident that the boron concentration in the transient liquid varied with time, indicating a dynamic phenomenon. At the solid/liquid interface, competitive boron-depletion and enrichment processes occurred simultaneously. On the one hand, the continuous boron diffusion back to the matrix caused the boron depletion, driven by the concentration gradient. On the other hand, the isothermal liquid solidification caused the boron enrichment of the residual liquid. According to the lever rule, the excess amount of boron between the solid and liquid (e.g. the difference between $C^{L\alpha}$ and $C^{\alpha L}$ in Fig. 2d) was rejected back to the liquid whenever new γ formed isothermally. The evidence from the microchemical data is that, in the composite, the enrichment process dominated the depletion process, resulting in the measured boron increase in the interlayer (Fig. 8). It should be noted that any boron increase in the interlayer would further enhance the concentration gradient, thus promoting the entire bonding process. Therefore, the boron enhancement in the interlayer, in fact, contributes another explanation for the conflict between the conventional kinetic models and the experimentally obtained bonding time [8, 12, 23].

5.2. The modified TLP bonding model

Based on the microchemical observations of boron redistribution during the TLP bonding in the composite, Fig. 2, which is the schematic illustration of the original mechanism of the TLP bonding process, was modified. Fig. 9 is a sketch of the proposed microstructural evolution for the Haynes 230/sapphire composite during TLP bonding, which includes the proposed stages of boron redistribution: (a) the initial assembly, (b) melting and widening of the interlayer, (c) isothermal solidification (liquid shrinkage), and (d) solidification of the "residual liquid" and boride precipitation in the matrix during cooling.

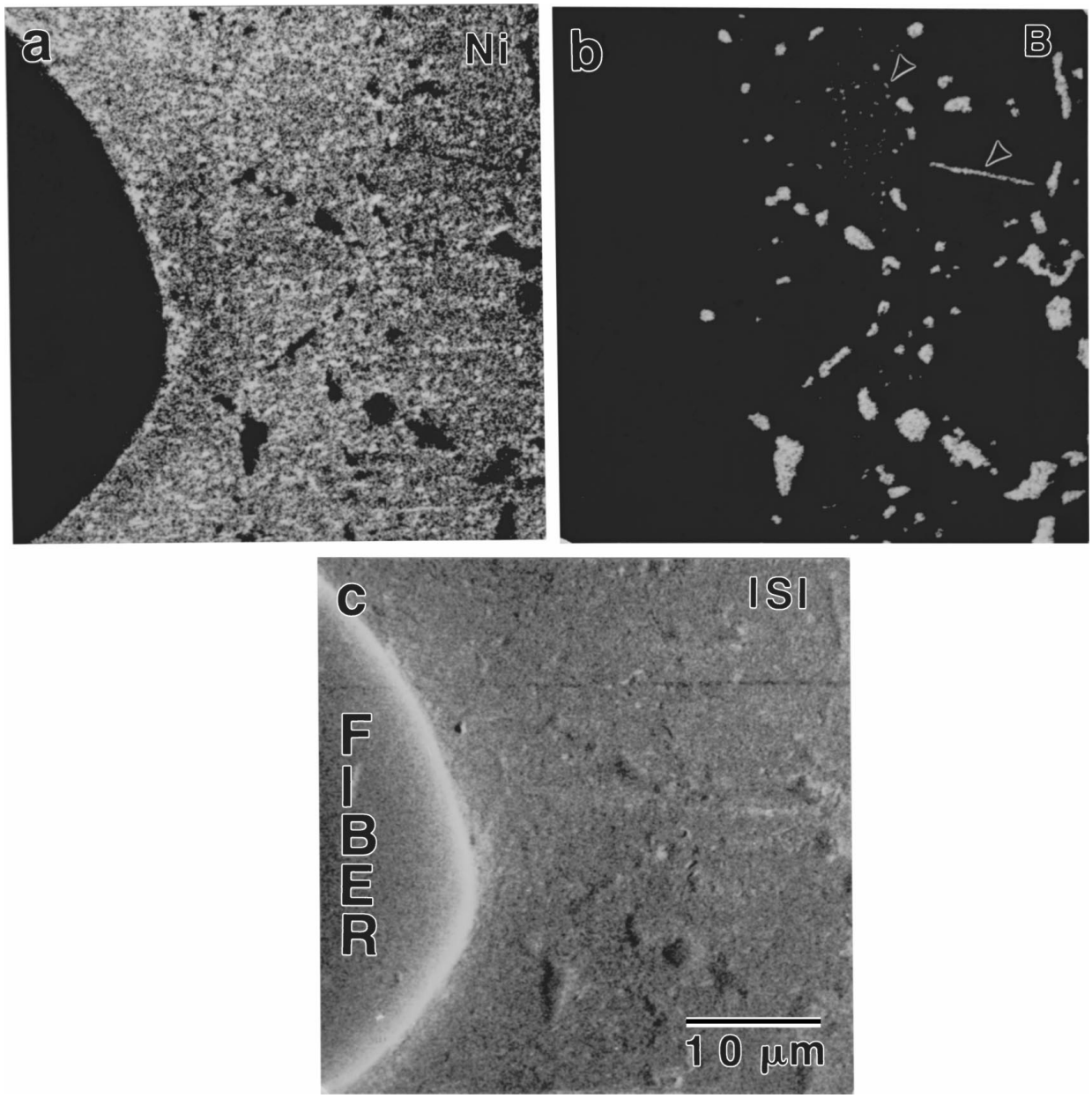

Figure 6 SIM images of an as-fabricated Haynes 230 superalloy/sapphire composite in a fiber/matrix interfacial area including region II: (a) Ni^+ map, (b) B^+ map, and (c) ISI topography. Note the fine boride precipitates can be clearly revealed in the B^+ map (arrowed), and Ni is depleted in the grain-boundary borides.

Boron concentration profiles across the composite for each stage of the bonding process are also depicted to illustrate the relative concentration gradients for adjacent regions. Note that the sapphire fiber is excluded intentionally. It should also be noted that the γ-phase region on the envisaged γ-boron phase diagram is extended greatly so that subtle changes in boron concentrations can be seen. In essence, the triangular γ region should be a narrow strip because it is assumed that the solubility of boron in γ is extremely low.

The important differences between the proposed TLP bonding mechanism (Fig. 9) and the existing models (such as that shown in Fig. 2) are as follows: for the investigated Haynes 230/sapphire composite (i) the concentration of the melting point depressant, boron, in the TLP *increased* with time during the isothermal solidification stage, (ii) the solubility of boron in γ is very low, resulting in extensive boride segregation to γ grain boundaries and fine boride precipitation within certain γ grains which were adjacent to the interlayer in the initial assembly, and (iii) because of the relatively high boron concentration in the interlayer, the TLP bonding was incomplete: boron was not consumed totally by the superalloy matrix within the two hours of bonding time and the post-bonding cooling stages, resulting in the formation of the "residual liquid" borides (region IV).

5.3. Microstructural modification

A principal conclusion of this study, therefore, is that the low solubility of boron in Ni (and in γ) and the relatively high boron concentration in the initial interlayer caused the heterogeneous microstructural evolution in the as-fabricated composite (Fig. 2). It is noted that the boron concentration is usually about 50–500 ppm in Ni-base superalloys. Boron usually segregates to grain boundaries, where it has positive effects on the creep strength of a superalloy. Although the mechanism of

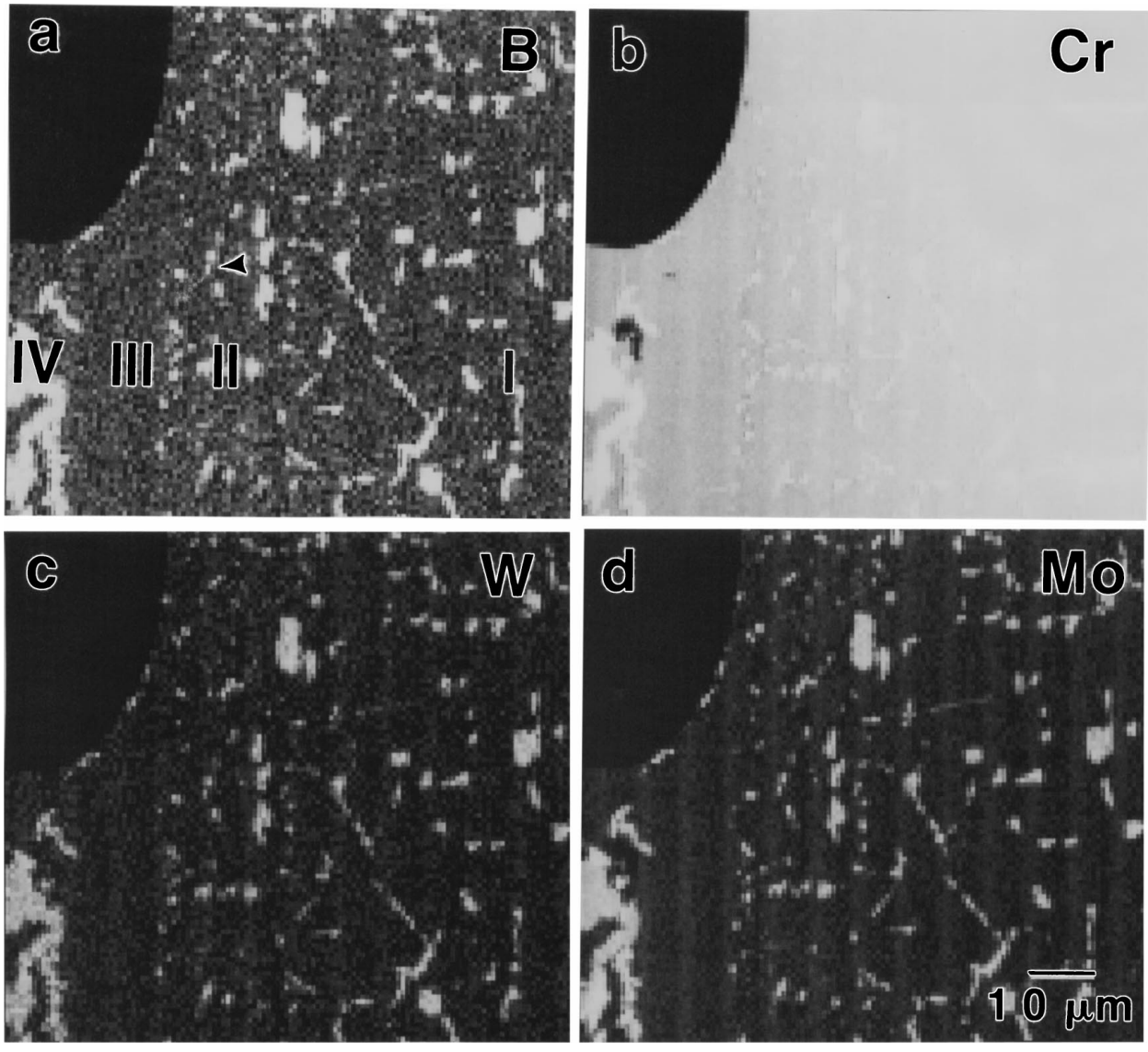

Figure 7 EPMA X-ray images of an as-fabricated Haynes 230 superalloy/sapphire composite in a fiber/matrix interfacial region including all the regions defined in Fig. 1: (a) B map, (b) Cr map, (c) W map, and (d) Mo map. Note that the fine boride precipitates in region II are barely revealed by EPMA.

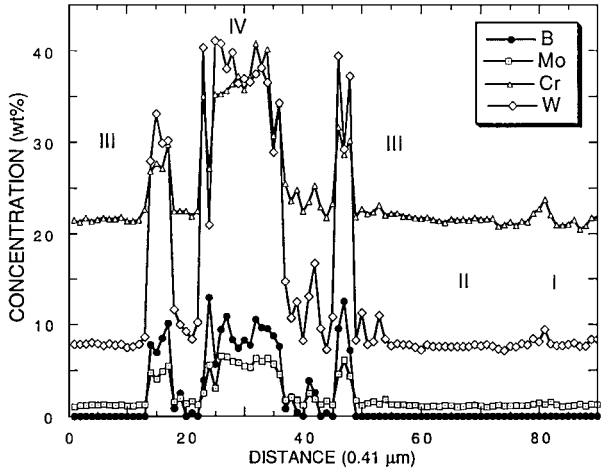

Figure 8 EPMA compositional profiles of B, Mo, Cr, and W across the matrix in an as-fabricated Haynes 230 superalloy/sapphire composite. It is clear that B, Mo, Cr, and W show similar segregation tendencies, consistent with the SIMS and EPMA maps (Figs 4–7).

how boron improves the creep resistance of a superalloy is not fully understood, it has been proposed that boron prevents the onset of grain boundary tearing and thus improves the rupture properties [28]. It is well known that segregation of boron to grain boundaries also improves the high-temperature mechanical properties of many intermetallic compounds such as Ni_3Al, $(Ni, Co)_3(Al, Ti)$, and other γ' phases [29, 30] but the exact mechanism is unknown. However, it is recognized that there is an optimum amount of boron to achieve the maximum strength in each case, beyond which more boron will cause lower strength. Therefore, the control of the boron content for TLP bonding is crucial, since there is nothing to be gained by improving the fabrication process if the net result is loss of high-temperature mechanical strength. To solve the problem of excess boron, two options are proposed: (1) reduce the amount of boron in the interlayer, and (2) increase the grain boundary area by either increasing

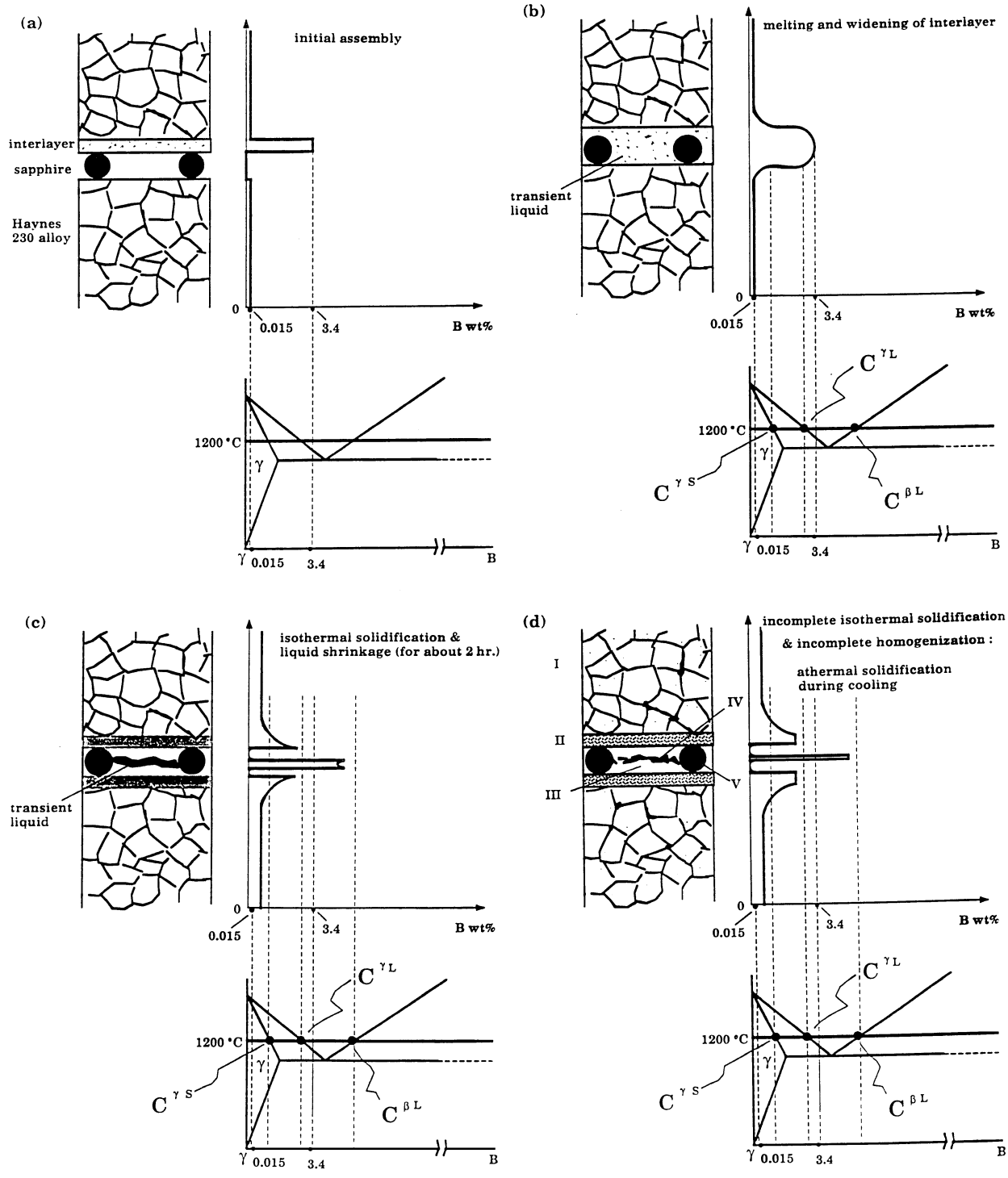

Figure 9 Schematic illustration of a modified mechanism of TLP bonding: (a) the initial composite assembly, (b) melting and widening of the interlayer, (c) isothermal solidification and shrinkage of the liquid, and (d) incomplete isothermal solidification and incomplete homogenization; athermal solidification of the residual liquid during cooling.

the amount of the matrix or reducing the initial grain size of the matrix [31].

It should be noted that the size of the inhomogeneous regions (i.e. regions II, III & IV in Fig. 1) is just slightly larger than the diameter of the sapphire fiber. A decrease in the width of the fibers will decrease the associated amount of interlayer required and, therefore, will decrease the total bonding time. A reduced-diameter fiber, in effect, has higher strength than a large-diameter fiber because the possibility of introducing surface flaws on a ceramic fiber during growth decreases as the surface area of the fiber decreases [32].

Theoretically, using TLP bonding, a homogeneous microstructure throughout the matrix can be obtained if a proper homogenizing treatment is given. Nakao [33] reported that a homogeneous structure was only reached in Alloy 713C after 225 h of holding time at 1100 °C. It is not surprising, therefore, that two hours of bonding time used in this study is insufficient to complete the bonding in the Haynes 230 composite.

Therefore, longer time is recommended to achieve homogenization although, as already noted this will result in significant grain growth.

Because boron has desirable effects on the properties of superalloys, and boron does not attack the sapphire fiber, it remains a promising candidate as a melting-point depressant for the composite. However, in order to obtain the same microstructure as that of the parent metal, it is necessary to develop new interlayers, more suitable for TLP bonding. The chemical compositions of such new interlayers would have to be very similar to those of parent metal.

6. Conclusions

1. This investigation indicates that the TLP bonding process proceeds under non-equilibrium conditions. Boron content increases not only in the solid matrix, but also in the liquid interlayer, while the conventional TLP models assume a decreasing amount of melting-point depressant in the interlayer.

2. Boron wets the grain boundaries, and supersaturates the matrix surrounding the interlayer, causing partial melting of this region.

3. Boron rejection during re-solidification causes increasing amounts of boron to diffuse back to the interlayer. This extra boron promotes the TLP bonding process, thus explaining why the experimentally obtained total bonding time is much shorter than the theoretically calculated value from the conventional kinetic models of TLP bonding.

4. A modified model for TLP bonding is proposed (Fig. 9). The major differences between the proposed model and the conventional models are as follows: (i) the concentration of the melting point depressant, boron, in the TLP increased with time during the isothermal solidification stage, (ii) the solubility of boron in γ is very low, resulting in extensive boride precipitation at γ grain boundaries (regions I & II) and fine boride precipitation within γ grains which were adjacent to the interlayer in the initial assembly (region II), and (iii) because of the relatively high boron concentration in the initial interlayer, the TLP bonding was not complete: boron was not consumed totally by the superalloy matrix within the two hours of bonding time and post-bonding cooling stages, resulting in the formation of the "residual liquid" borides (region IV).

5. Reduced-diameter fibers will reduce the associated amount of interlayer required, and thus will reduce the total bonding time. In addition, a smaller-diameter fiber has higher strength due to reduced possibility of introducing surface flaws; therefore, having a higher fiber reinforcing (or strengthening) effect in the composite.

6. The as-fabricated composite has a heterogeneous microstructure. However, the problem can be overcome by reducing the amount of boron in the interlayer and by increasing the homogenization time. A smaller starting grain size for the superalloy matrix is also recommended.

Acknowledgements

The authors gratefully acknowledge Rockwell International Corporation for provision of the composite materials, and wish to thank Drs. C. C. Bampton and J. R. Porter of Rockwell for valuable discussions. This work was funded by NSF grant DMR 9111839.

References

1. C. C. BAMPTON and M. A. CUNNINGHAM, Patent: EP0502426, European Patent, 27 February (1992).
2. R. L. MEHAN and M. J. NOONE, in "Metallic Matrix Composites," Vol. 4, edited by K. G. Kreider (Academic Press, New York, 1974) p. 159.
3. V. SRINIVASAN, *Journal of Metals* **46**(12) (1994) 34.
4. S. KOLLI, PhD dissertation, Ohio State University, Columbus, OH, 1991.
5. C. C. BAMPTON and M. A. CUNNINGHAM, "HIPTEMP Review 1992, Compressor/Turbine Materials (Metal/lntermetallic Matrix Composites)" Vol. 2, (NASA Conference Publication, 1992) p. 36.1.
6. T. J. LIENERT, C. T. LANE and J. W. GOULD, "ASM Handbook No. 6, Welding, Brazing, and Soldering" (ASM International, Materials Park, OH, 1993) p. 554.
7. Z. LI, Y. ZHOU and T. H. NORTH, in Proceedings of Cancom '93, the Second Canadian International Composites Conference and Exhibition, Ottawa, Ontario, Canada, 1993, p. 1017.
8. W. D. MACDONALD and T. W. EAGAR, *Ann. Rev. Mater. Sci.* **22** (1992) 23.
9. L. P. DING, F. Z. YAO and Y. Q. GUO, *Hanjie Xuebao (Trans. China Weld. Inst.)* **3**(3) (1982) 21.
10. T. YAMADA, *J. Japan. Weld. Soc.* **57**(7) (1988) 32.
11. W. F. GALE and E. R. WALLACH, "Euromat '91, Advanced Processing," Vol. 1, (The Institute of Materials, London, UK, 1992) p. 391.
12. J. P. JUNG, B. Y. LEE and C. S. KANG, in Proceedings of the Conference on International Trends in Welding Science and Technology, Tennessee, USA, 1992 (ASM International, Materials Park, OH, 1993) p. 1101.
13. Y. ZHENG, L. ZHAO and K. TANGRI, *J. Mater. Sci.* **28** (1993) 823.
14. Y. NAKAO, in Proceedings of the Conference on Stainless Steels '91 (Chiba, Japan 1991) Vol. 2, p. 975.
15. W. Y. KIM, C. Y. KANG and S. Y. PARK, *J. Korean Institute of Metals and Materials* **29**(12) (1991) 1274.
16. D. V. DUNFORD and P. G. PARTRIDGE, *J. Mater. Sci.* **27** (1992) 3389.
17. R. A. RICKS, G. J. MAHON and P. J. WINKLER, in Proceedings of the Conference on the Processing, Properties and Applications of Metallic and Ceramic Materials (Institute of Materials, London, UK, 1992) Vol. II, p. 1025.
18. D. W. LIVERSEY and N. RIDLEY, in Proceedings of the Conference on Diffusion Bonding, Cranfield, UK, 1990 (Elsevier Science Publishers, London, UK, 1991) Vol. 2, p. 83.
19. W. D. MACDONALD and T. W. EAGAR, in Proceedings of the Conference on International Trends in Welding Science and Technology, Tennessee, USA, 1992 (ASM International, Metals Park, OH, 1993) p. 1083.
20. E. R. WALLACH and P. YAN, *Intermetallics* **1** (1993) 83.
21. S. V. OREL, L. C. PAROUS and W. F. GALE, in Proceedings of the Conference on Advanced Joining Technologies for New Materials (American Welding Society, 1994) Vol. II, p. 5.
22. D. S. DUVALL, W. A. OWCZARSKI and D. F. PAULONIS, *Welding J.* **53** (1974) 203.
23. I. TUAH-POKU, M. DOLLAR and T. B. MASSALSKI, *Metall. Trans.* **19A** (1988) 675.
24. R. LEVI-SETTI, J. M. CHABALA, K. L. GAVRILOV, J. LI, R. MOGILEVSKY and K. K. SONI, in "Scanning Microscopy," edited by O. Johari (Scanning Microscopy Intl., IL, 1994) p. 1161.
25. D. B. WILLIAMS, K. K. SONI, M. W. TSENG, J. M. CHABALA and R. LEVI-SETTI, *J. Microsc.* **169** (1993) 163.
26. K. K. SONI, J. M. CHABALA, R. MOGILEVSKY, R. LEVI-SETTI, M. W. TSENG and D. B. WILLIAMS, *Journal of Metals* **45**(3) (1993) 29.
27. P. K. LIAO and K. E. SPEAR, "ASM Handbook No. 3, Alloy Phase Diagrams," Vol. 3, (ASM International, Materials Park, OH, 1992) p. 2.83.

28. E. W. ROSS and C. T. SIMS, in "Superalloy II," edited by C. T. Sims (John Wiley & Sons, New York, 1987) p. 112.
29. N. S. STOLOFF, *International Materials Reviews* **34** (1989) 153.
30. J. FANG and E. M. SCHULSON, *Mater. Sci. & Eng.* **A152** (1992) 138.
31. J. KOKAWA C. H. LEE and T. H. NORTH, *Metall. Trans.* **22A** (1991) 1627.
32. D. W. RICHERSON, "Modern Ceramic Engineering," 2nd ed. (Marcel Dekker, New York, 1992) p. 162.
33. Y. NAKAO, in Proceedings of Japan-US Seminar on Superalloys (Japan Institute of Metals, 1985) p. 231.

Received 23 December 1998
and accepted 21 April 1999